Atoms-to-Circuits Simulation Investigation of CNT Interconnects for Next Generation CMOS Technology

Jaehyun Lee[1*], Jie Liang[2], Salvatore M. Amoroso[3], Toufik Sadi[1,4], Liping Wang[3], Plamen Asenov[3], Andrew Pender[3], Dave T. Reid[3], Vihar P. Georgiev[1], Campbell Millar[3], Aida Todri-Sanial[2], and Asen Asenov[1], *Fellow IEEE*

[1]*School of Engineering, University of Glasgow, Glasgow, Scotland, UK, *Jaehyun.Lee@glasgow.ac.uk*
[2]*CNRS-LIRMM, University of Montpellier, Montpellier, France*
[3]*Synopsys Inc., Glasgow, Scotland, UK*
[4]*Department of Neuroscience and Biomedical Engineering, Aalto University, Helsinki, Finland*

***Abstract*—In this study, we suggest a hierarchical model to investigate the electrical performance of carbon nanotube (CNT)-based interconnects. From the density functional theory, we have obtained important physical parameters, which are used in TCAD simulators to obtain the RC netlists. We then use these RC netlists for the circuit-level simulations to optimize interconnect design in VLSI. Also, we have compared various CNT-based interconnects such as single-walled CNTs, multi-walled CNTs, doped CNTs, and Cu-CNT composites in terms of conductivity, ring oscillator delay, and propagation time delay.**

***Keywords*—Density Functional Theory (DFT); circuit simulation; hierarchical models; interconnects; carbon nanotubes (CNTs); Cu-CNT composites;**

I. Introduction

Complementary Metal–Oxide–Semiconductor (CMOS) scaling dictates a shrinking in interconnect wiring size, resulting in increased Cu resistivity (mainly due to surface roughness and grain boundary scatterings) and decreased reliability (mainly limited by electro-migration) [1-3]. At the current technology generation, interconnect delay is comparable to transistor delay, which will represent a major limit to next-generation circuit performance [4].

Carbon NanoTubes (CNTs) exhibit small effective transport masses and a nearly one-dimensional (1-D) ballistic transport, which results in high electrical and thermal conductivities. Moreover, very high ampacity (100 times the value of Cu [5]) and excellent mechanical properties make them a promising candidate for replacing Cu interconnects. Manufacturability, process yields and variability of metallic CNT remain major issues [6].

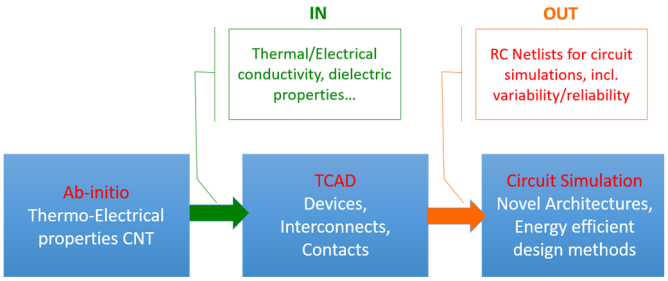

Fig. 1. Multiscale Atoms-to-Circuits Simulation Flow.

In this work, we present a hierarchical simulation approach to studying of CNT-based interconnect performance [7-9]. The transport properties of CNT interconnects are first evaluated by *ab-initio* methods. The extracted material properties are then used in 3D TCAD simulations to extract resistance and capacitance (RC) for complex interconnects systems. These interconnect RC netlists are then used in circuit-level simulations for design optimization. The proposed multi-scale simulation flow is illustrated in Fig.1.

II. Methodology

A. Ab-inito simulation

We have used the Density Functional Theory (DFT) – Non-Equilibrium Green's Function (NEGF) framework implemented in Atomistix ToolKit (ATK) [10] to obtain physical material parameters such as the ballistic conductance. Firstly, we have performed a geometrical optimization for single-walled CNTs (SWCNTs), multi-walled CNTs (MWCNTs), iodine-doped CNTs and Cu-CNT composites. All atoms are fully relaxed until maximum force becomes less than 0.01 eV/Ang. Fig.2 shows the optimized atomic structures of iodine-doped MWCNT (15,0)(24,0) and Cu-CNT(6,0) composite. In order to minimize the lattice mismatch for the Cu-CNT(6,0) composite, the transport direction of Cu is set to $[11\bar{2}]$.

After calculating the ballistic conductance (G_{bal}) with the DFT-NEGF approach, a mean free path approximation is adopted to describe the phonon scattering effects. The diffusive conductance (G_{dif}) can be calculated using following equation:

$$G_{dif} = G_{bal}\left(1+\frac{L}{\lambda}\right)^{-1}, \quad (1)$$

where L and λ are the interconnect length and the mean free path, respectively.

The quantum capacitance (C_Q) can also be calculated from the density-of-states (DOS) obtained from the DFT calculations, using the following equation [11]:

$$C_Q = \frac{e^2}{4kT}\int DOS(E)\,\mathrm{sech}^2\frac{E}{2kT}dE, \quad (2)$$

where e, k, and T are the elementary charge, Boltzmann constant, and temperature, respectively.

B. TCAD & circuit simulation

A finite-difference approach is adopted to solve the Laplace equations for RC extraction in complex interconnect structures such as the inverter:

$$\nabla\varepsilon\nabla\psi = 0 \text{ for an insulator} \quad (3)$$

$$\nabla k\nabla\psi = 0 \text{ for a metal,} \quad (4)$$

where ε, k, and ψ are permittivity, conductivity, and potential, respectively.

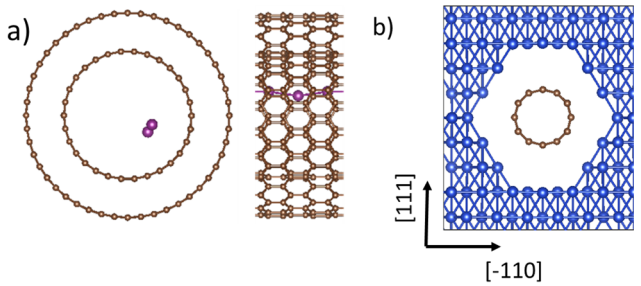

Fig. 2. Atomistic structures of a) iodine doped MWCNT (15,0)(24,0) and b) Cu-CNT (6,0) composite. Brown, blue, and vilolet spheres indicate the carbon, copper, and iodine atoms, respectviley.

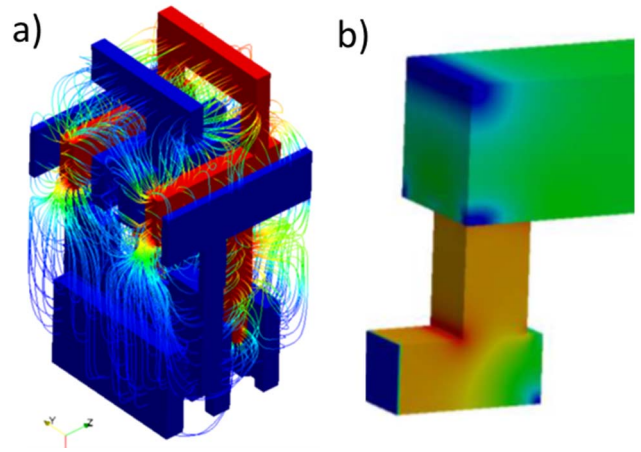

Fig. 3. (a) 3D TCAD Capacitance, where the electric field streamlines highlight the cross-talk between interconnects. (b) Resistance simulation detail, where the current density flow highlights the interconnects critical hot-spots.

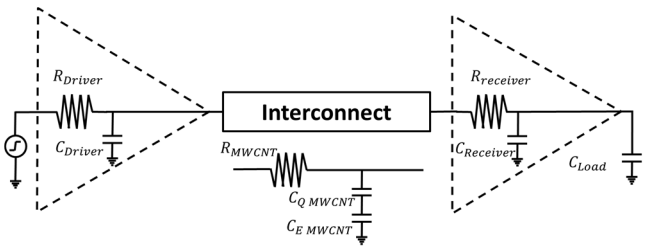

Fig. 4. Schematic representation of a typical interconnect

Fig. 3 shows the 3D TCAD simulation output for a 14nm CMOS inverter highlighting the cross-talk between lines up to the M2 interconnect level. Advanced models for conductivity and capacitance of both Cu and CNT are implemented using *ab-initio* results. Extracted RC netlists are provided in a SPICE-like format for the next stage.

Fig. 4 describes the circuit of the typical interconnect with driver and receiver buffers. The buffer gates are implemented with CMOS 45nm technology node. R_{driver}, C_{driver} and C_{load} are assumed to be 24 kΩ, 450 aF and 10 fF, respectively. For the circuit simulation, we have considered C_Q, but the total capacitance of the interconnects (C_W) remains quasi-constant because the classical electrostatic capacitance (C_E) is much lower than C_Q in this technology:

$$C_W = \left(C_Q^{-1} + C_E^{-1}\right)^{-1}. \quad (5)$$

We also considered doping effects that increase the number of conducting channels (N_C). From the DFT simulations, we have found that N_C can be increased from 2 up to 8 if somehow the Fermi-level is shifted by ± 1.0 eV relative to the Fermi-level of the pristine CNT. N_C can be obtained from G_{bal}:

$$N_C = \frac{G_{bal}}{G_0}, \quad (6)$$

where G_0 is the quantum conductance.

III. Simulation Results

The calculated ballistic conductance and quantum capacitance are summarized in Table 1. The former was normalized to the cross-sectional area, and the latter to the area and length. In this study, the area of CNTs is assumed to be

$$A = \frac{\sqrt{3}}{2}(D_{CNT} + d_{VDW})^2, \quad (7)$$

where the van der Waals distance (d_{VDW}) is 0.34 nm and D_{CNT} is the diameter of CNT. As can be seen from this table, G_{bal} of CNTs is smaller than those of bulk Cu. It means that although CNTs have ideally zero effective masses (high mobility), the resistance is still larger than bulk Cu. In terms of the capacitance, however, it is obvious that CNTs have a clear advantage.

TABLE I. Ballistic Conductance and Quantum Capacitance of Each Material

	Ballistic Conductance (mS/nm^2)	Quantum Capacitance (aF/nm^3)
SWCNT(24,0)	0.033	0.132
Doped	0.054	0.251
MWCNT (15,0)(24,0)	0.065	0.206
Doped	0.089	0.418
Cu-CNT(6,0) composite	0.582	4.743
Bulk Cu [11-2]	0.785	6.110

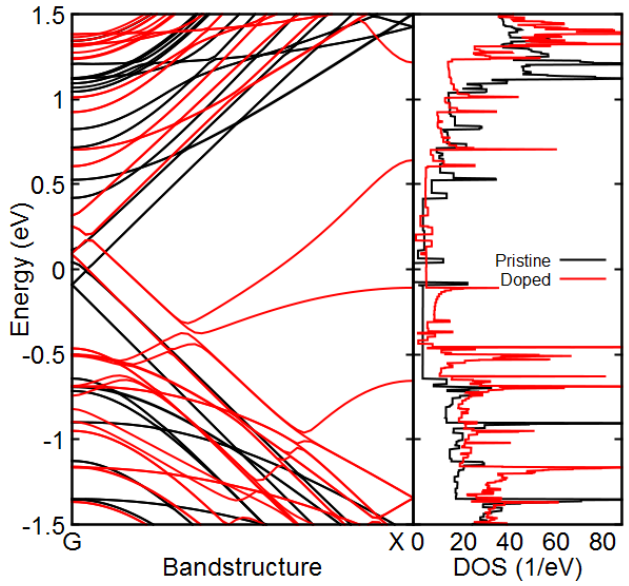

Fig. 5. Band structures and DOSs of pristine (black) and doped (red) MWCNT(15,0)(24,0). Fermi-level is set to 0.0 eV.

To enhance the ballistic conductance of CNTs, we have considered the MWCNTs, the doped CNTs, and Cu-CNT composites. Generally, MWCNTs have higher G_{bal} and C_Q than SWCNTs when they have the same D_{CNT}. This is because each shell of MWCNTs is independent, and reducing the empty space inside the tube allows the conducting channel to be used more efficiently. In the case of the iodine-doped CNTs, DOS and the number of conducting channel near the Fermi-level increases as can be seen in Fig. 5 thanks to the Fermi-level shift by dopants. The Cu-CNT composites have the material advantages of both Cu and CNT. They have larger G_{bal} than CNTs, and smaller C_Q than bulk Cu.

Fig. 6 illustrates the dependence of the diffusive conductivity of pristine and iodine-doped CNTs, Cu-CNT composites, and bulk Cu on the interconnect length. When the interconnect length is shorter than 1 μm, bulk Cu, which has the largest value of the ballistic conductance in Table 1, has the largest conductivity. However, when the interconnect length is longer than 1 μm, the iodine-doped MWCNT(15,0)(24,0) shows the best performance because the mean free path of CNTs ($1000 \times D_{CNT}$ nm) is longer than Cu (40 nm). We have also found that doped SWCNTs and MWCNTs have a larger conductivity than pristine SWCNTs and MWCNTs, respectively, thanks to their large N_C. The Cu-CNT composite interconnects have a higher conductivity than CNTs in the short interconnects (L < 500 nm) and a higher conductivity than bulk Cu in the long interconnects (L > 500 nm).

Fig. 7 shows the output voltage waveform in an interconnect within a 17-stage ring oscillator. We have compared the ring oscillator delay (ROD) with an ideal material, Cu, and CNTs. In the case of the ideal interconnects, since there is no propagation time delay in the interconnect, ROD is only limited by the CMOS gate delay. As shown in this figure, the CNT

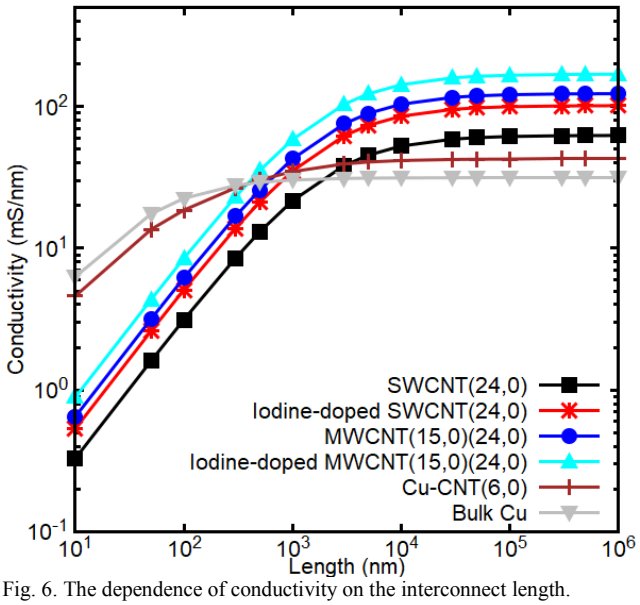

Fig. 6. The dependence of conductivity on the interconnect length.

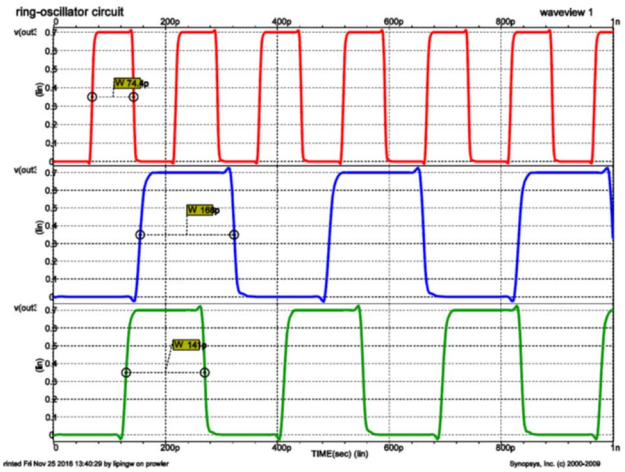

Fig. 7. 17-stage Ring-Oscillator circuit simulation comparison between ideal (top), Cu (middle) and CNT (bottom) interconnects.

interconnect shows a performance closer to the ideal interconnect compared to the Cu interconnect.

Fig. 8. describes the dependence of the propagation time delay ratio of MWCNT interconnects with various D_{CNT}^{max} s, where D_{CNT}^{max} is their outermost shell diameter. The propagation time delay ratio is calculated by the ratio of propagation delay based on the pristine MWCNT [6, 7]. In this study, we assumed that the MWCNT is filled with shells until its diameter is smaller than $\frac{D_{CNT}^{max}}{2}$, and each shell of the doped MWCNT has the same N_C. As shown in these figures, we have observed that as L increases, doping is more effective in reducing the propagation

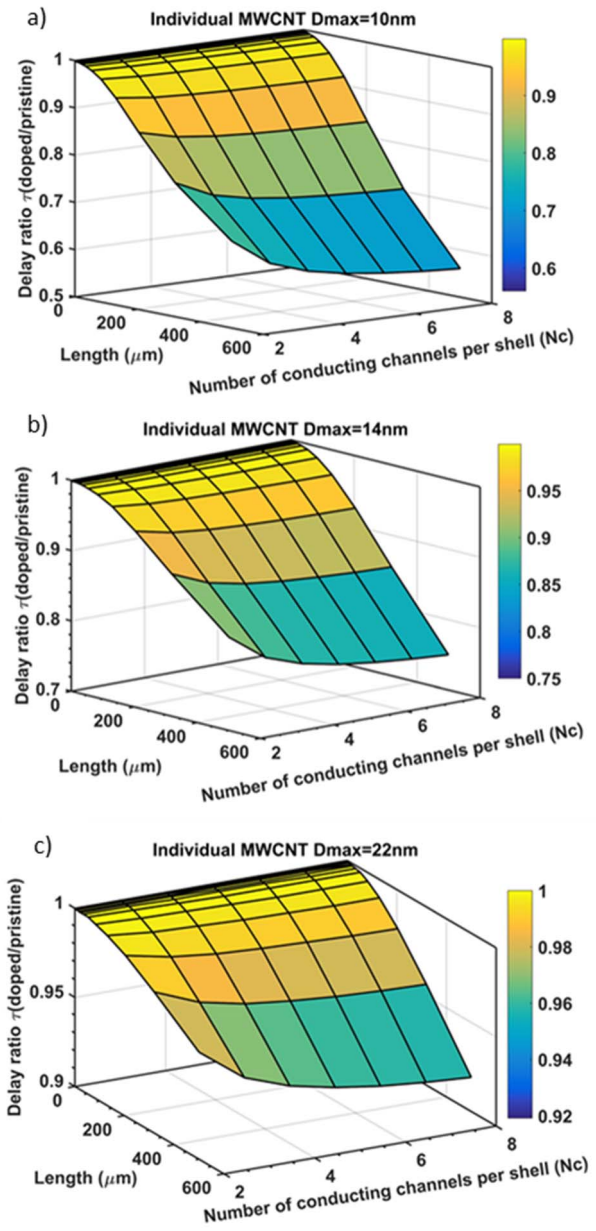

Fig. 8. The dependence of the delay ratio of MWCNT interconnects with D_{CNT}^{max} = a) 10 nm, b) 14 nm, and c) 22 nm on the interconnect length and the number of conducting channel per shell.

delay. Moreover, dopants in MWCNT interconnects with D_{CNT}^{max} = 10, 14, and 22 nm reduce the propagation delay by 10, 5 and 2 %, respectively, when L = 600 μm. Because increasing D_{CNT}^{max} increases the number of shells (N_{sh}) and the total number of the conducting channels ($N_c^{totla} = N_{sh} \times N_c$), the effect of doping is reduced.

IV. Conclusions

We have presented a multiscale simulation flow to allow the design-technology co-optimization of CNT-based interconnect technologies. We have benchmarked CNT performances vs. Cu. We have demonstrated the impact of iodine doping and Cu-CNT composites on CNT interconnects performance

Acknowledgment

This work is supported by EU H2020 CONNECT project under grant agreement No. 688612, http://www.connecth2020.eu/.

References

[1] W. Wu, S. H. Brongersma, M. V. Hove and K. Maex, "Influence of sruface and grain-boundary scattering on the resisitvity", *Appl. Phys. Lett.,* vol. 84, no. 15, pp. 2838-2840, 2004.

[2] W. Steinhögl, G. Schindler, G. Steinlesberger, M. Traving, and M. Engelhardt, "Comprehensive study of the resistivity of copper wires with lateral dimensions of 100 nm and smaller", *J. Appl. Phys.,* vol. 97, 023706, 2005.

[3] E. T. Ogaw, K. Lee, V. A. Blaschke, and P. S. Ho, "Electromigration Reliability Issues in Dual-Damascene Cu Interconnections", *IEEE Trans. Rel*., vol. 51, no. 4, pp. 403-419, 2002.

[4] International Technology Roadmap for Semiconductors (ITRS) 2.0, 2015 Edition

[5] C. Subramaniam, T. Yamada, K. Kobashi, A. Sekiguchi, D. N. Futaba, M. Yumura and K. Hata, "One hundred fold increase in current carrying capacity in a carbon nanotube–copper composite" *Nat.Commun.* vol. 4, 2202, 2013.

[6] A. Todri-Sanial, J. Dijon and A. Maffucci, "Carbon Nanotube Interconnects: Process, Design and Applications*",* Springer, 2016.

[7] A. Todri-Sanial, R. Ramos, H. Okuno, J. Dijon, A. Dhavamani, M. Wislicenus, K. Lilienthal, B. Uhlig, T. Sadi, V. P. Georigev, A. Asenov, S. M. Amoroso, A. R. Brown, A. Pender, C. Millar, F. Motzfeld, B. Gotsmann, J. Liang, G. Goncalves, N. Rupesinghe, and K. Teo, "A Survey of Carbon Nanotube Interconnects for Energy Efficient Integrated Circuits", IEEE Circuits and Systems Magazine, vol. 17, pp. 47-62, 2017.

[8] A. Naeemi and J. D. Meindl, "Compact Physical Models for Multiwall Carbon-Nanotube Interconnects", *IEEE Electron Device Lett*., vol. 27, no. 5, pp. 338-340, 2006.

[9] H. Li, W. Yin, K. Banerjee and J. Mao, "Circuit modeling and performance analysis of multi-walled carbon nanotube interconnects.", *IEEE Trans. on Electron Devices*, vol. 55, no. 6, pp. 1328-1337 2008.

[10] Atomistix Tool Kit (2016.4), QuantumWise A/S

[11] C. Zhan, J. Neal, J. Wu and D. Jiang, "Quantum Effects on the Capacitance of Graphene-Based Electrodes", *J. Phys. Chem.,* vol. 119, no. 39, pp. 22297-22303, 2015.